# THE EFFECTS OF GRAPHENE SIZE AND MORPHOLOGY ON DAMPING PROPERTIES OF POLYMER NANOCOMPOSITES

A Thesis

by

SEVKETCAN SARIKAYA

Submitted to the Office of Graduate and Professional Studies of
Texas A&M University
in partial fulfillment of the requirements for the degree of

MASTER OF SCIENCE

| | |
|---|---|
| Chair of Committee, | Mohammad Naraghi |
| Committee Members, | Ramesh Talreja |
| | Terry Creasy |
| Head of Department, | Ibrahim Karaman |

August 2019

Major Subject: Materials Science and Engineering

# ABSTRACT

This work investigates the improvements in damping performance of polymer nanocomposites with graphene inclusions by employing interfacial slippage mechanisms between filler and matrix. The damping improvement to the nanocomposite benefits from the large interfaces of the matrix-graphene or graphene layers between which frictional sliding occurs to dampen vibration. In particular, we have studied the effect of morphology and particle size of graphene on the damping properties of a polymer system. To this end, two types of graphene nanoparticles with different morphologies and aspect ratios were used as fillers in polystyrene matrix: single layer graphene (SLG) and graphene nanoparticles (GNP). The dynamic mechanical behavior of the two nanocomposite systems was studied. A micromechanical model, based on shear lag analysis which captures the load transfer between nanoparticles and matrix was also used to acquire a deeper understanding of the damping mechanism. The results pointed to a considerable effect of graphene morphology in facilitating (or delaying) the interfacial failure, leading to enhanced (or reduced) damping performance. The combined modeling-experimental work suggests that the wrinkles on the surface of SLG, caused by its low bending stiffness, are a major player in enhancing the interfacial shear strength (IFSS) between the polymer and the graphene, leading to ~15x improvement in IFSS.

# DEDICATION

Dedicated to my mother and father,

and loved ones

# ACKNOWLEDGEMENTS

I would like to express my appreciation and thanks to my advisor, Dr. Mohammad Naraghi, for his guidance and support throughout the whole period of my research. I would also like to thank my committee members, Dr. Ramesh Talreja and Dr. Terry Creasy for serving as my committee members and their valuable suggestions and comments.

I would like to extend my sincere thanks to Dr. Todd Henry for his effort and technical support for the experiments. I acknowledge the support of DOD— United States Army Research Laboratory (USARL) and TAMU Materials Characterization Facility.

I would like to thank everyone in Nanostructured Materials Lab, Dr. Ahmad Amiri, Dr. Aniruddh Vashisth, Yijun Chen, Jamshid Kavosi, Kai Morikawa, Sumit Khatri, and Taimoor Ashraf not only for their technical help and advice but also their friendship. Moreover, thanks should also go to Kaan Sel for a great friendship which was built in a short period of time.

I would also like to extend my deepest gratitude to the Turkish Ministry of National Education for the financial support which grants me to study in the U.S. Otherwise, this thesis would not have been possible.

Lastly, I would like to express my deepest appreciation to my mother and father who always encourage and support me for every decision I make. I would not have achieved anything without their continuous unwavering support.

# CONTRIBUTORS AND FUNDING SOURCES

## Contributors

This work was supervised by a thesis committee consisting of Dr. Mohammad Naraghi (advisor) and Dr. Terry Creasy of the Department of Material Science Engineering and Dr. Ramesh Talreja of the Department of Aerospace Engineering.

The Dynamic Mechanical Analysis (DMA) data for Chapter 4 was collected by Dr. Todd Henry in the Army Research Lab. Texas A&M University Materials Characterization Facility (MCF) is acknowledged for the SEM imaging facility.

All other work conducted for the thesis was completed by the student independently.

## Funding Sources

Graduate study was financially supported by a fellowship of the Turkish Ministry of National Education.

This work was also made possible in part by DOD— United States Army Research Laboratory (USARL) under Grant Number W911NF-16-2-0238. Its contents are solely the responsibility of the authors and do not necessarily represent the official views of the USARL.

# NOMENCLATURE

| | |
|---|---|
| CNTs | Carbon Nanotubes |
| DMA | Dynamic Mechanical Analysis |
| DMF | Dimethylformamide |
| GNP | Graphene Nanoplatelet |
| PC | Polycarbonate |
| PS | Polystyrene |
| RVE | Representative Volume Element |
| SLG | Single Layer Graphene |
| SWCNTs | Single-wall Carbon Nanotubes |
| $T_g$ | Glass Transition Temperature |
| $\tau$ | Interfacial Shear Stress |

TABLE OF CONTENTS

Page

ABSTRACT ..... ii

DEDICATION ..... iii

ACKNOWLEDGEMENTS ..... iv

CONTRIBUTORS AND FUNDING SOURCES ..... v

NOMENCLATURE ..... vi

TABLE OF CONTENTS ..... vii

LIST OF FIGURES ..... ix

LIST OF TABLES ..... xi

1. INTRODUCTION ..... 1

2. BACKGROUND AND LITERATURE REVIEW ..... 3

2.1. Damping in Polymer Nanocomposites ..... 3
2.2. Graphene as a Nanofiller ..... 5
2.3. Graphene Reinforced Polymer Nanocomposites ..... 6

3. EXPERIMENT AND MODEL DESIGN ..... 12

3.1. Fabrication of Graphene Nanocomposites ..... 12
3.2. Mechanical and Material Characterization of Graphene Nanocomposites ..... 13
3.3. Micromechanical Model of Damping Characterization ..... 14

4. RESULTS AND DISCUSSION ..... 19

4.1. Morphological Insight of Graphene and Graphene Nanocomposites ..... 19
4.2. Damping Ratio and Storage Modulus of PS/GNP ..... 21
4.3. Comparison of Micromechanical Model and Experimental Results ..... 25
4.4. Damping Ratio and Storage Modulus of PS/SLG ..... 31
4.5. The Effect of Graphene Morphology on Damping ..... 33

5. CONCLUSION AND FUTURE DIRECTIONS ..... 36

5.1. Conclusion....36
5.2. Future Directions....37

REFERENCES....38

LIST OF FIGURES

Page

Figure 1. The design of rotor hub of Boeing Model 360 helicopter with polymeric damper. Reprinted from [4] with permission. ..... 2

Figure 2. Commonly used reinforcements in polymer nanocomposites and their surface area/volume relations. Reprinted from [12] with permission. ..... 3

Figure 3. Damping results of pure PS and CNT reinforced PS nanocomposites as a function of strain. Reprinted from [14] with permission. ..... 5

Figure 4. 2D structure of graphene might be seen as a source of all carbon-based fillers. Reprinted from [26] with permission. ..... 7

Figure 5. a) Storage modulus and b) damping (tanδ) values of functionalized graphene reinforced polystyrene nanocomposites as a function of temperature. Reprinted from [32] with permission. ..... 9

Figure 6. Three main dispersion behaviors occurring in nanofiller reinforced polymer nanocomposites. Reprinted from [39] with permission. ..... 10

Figure 7. The schematic demonstration of the production of GNP/PS and SLG/PS nanocomposites via a solution mixing process. ..... 13

Figure 8. Representative Volume Element (RVE) of a graphene flake embedded in a polymer matrix ..... 15

Figure 9. Schematic demonstration of how debonding and friction occur in polymer nanocomposites ..... 16

Figure 10. The SEM images of a) as received GNP, b) as received SLG ..... 20

Figure 11. The SEM images of the cross-section of a) PS/GNP and b) PS/SLG nanocomposites perpendicular to the extrusion direction. Images are taken from fracture surfaces perpendicular to the extrusion direction. ..... 20

Figure 12. The experimental DMA results of the storage modulus of neat PS and PS/GNP nanocomposite with a function of dynamic strain ..... 22

Figure 13. The experimental DMA results of a) tanδ of neat PS and PS/GNP nanocomposite with a function of dynamic strain ..... 23

Figure 14. Damping of PS/CNT nanocomposites for different CNT weight percentages. In the low strain regime, there is no slippage filler/polymer slippage, which is not a case in the graphene/polymer system. Reprinted from [47] with permission. ..... 24

Figure 15. The comparisons of the model and experimental damping (tanδ) values ..... 27

Figure 16. The distribution of the interfacial shear stress on a graphene flake as a function of the graphene aspect ratios. The shear stress and distance are normalized by an applied stress and graphene length, respectively. The applied strain is 0.3%. ..... 28

Figure 17. The distribution of the strain on a graphene flake as a function of the graphene aspect ratios. Strain and distance are normalized by an applied strain and graphene length, respectively. The applied strain is 0.3%. ..... 30

Figure 18. The experimental storage modulus of PS/SLG and PS with a function of dynamic strain ..... 31

Figure 19. The experimental tanδ values of PS/SLG and PS with a function of dynamic strain ..... 33

Figure 20. The schematic illustration of the forces influencing the a) PS-GNP and b) PS-SLG interface ..... 35

LIST OF TABLES

Page

Table 1. Input data for the micromechanical damping model.....25

# 1. INTRODUCTION

Damping undesirable vibrations is essential for the safe operation of many devices for mitigating instabilities, increasing service life and reduced maintenance cost [1,2]. Aerospace structures such as rotor shafts and wings face undesirable vibrations, which may even cause catastrophic failures [3]. Some vehicles also are limited in performance due to aeroelastic stability. Structural designers commonly employ polymeric dampers to structures benefiting from the inherent viscous damping mechanism in polymers to extract mechanical energy from a vibrating system [4,5]. Although this approach suppresses structural vibrations, it increases structural complexity and maintenance requirements, and adds extra weight [6,7]. The typical current polymer damping configurations in a helicopter rotor hub are shown in Figure 1. Moreover, viscoelastic polymeric dampers have limited damping capability, which may be increased only at elevated temperatures but at the cost of stiffness [8]. Increased system damping for no change in stiffness would increase the performance of the forward flight speed of tiltrotor aircraft [9]. Therefore, the current helicopter rotor hub designs are still looking for a reliable solution that ensures enhanced flights and operations.

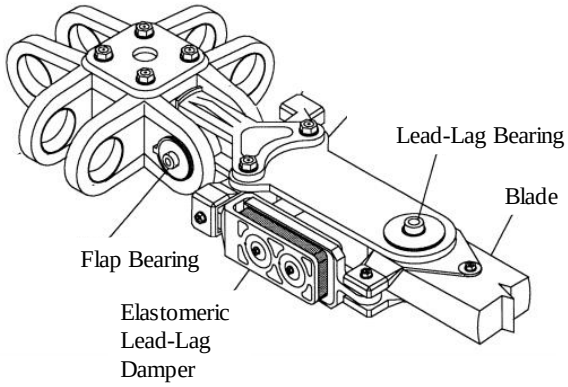


**Figure 1.** The design of rotor hub of Boeing Model 360 helicopter with polymeric damper. Reprinted from [4] with permission.

# 2. BACKGROUND AND LITERATURE REVIEW

## 2.1. Damping in Polymer Nanocomposites

The damping performance of polymers can be enhanced by adding nanofillers [10]. The filler-matrix interface would help surpass structural vibrations and dissipate energy thanks to the friction occurring on the filler/matrix interface [11]. Commonly used nanofiller geometries in polymer nanocomposites are shown in Figure 2 with their surface area/volume relations. Therefore, the abundance of filler-matrix interfaces, owed to the small dimensions of the nanofibers, can lead to inherent and considerable structure damping of vibration without a weight penalty or adverse effects in any other mechanical property.

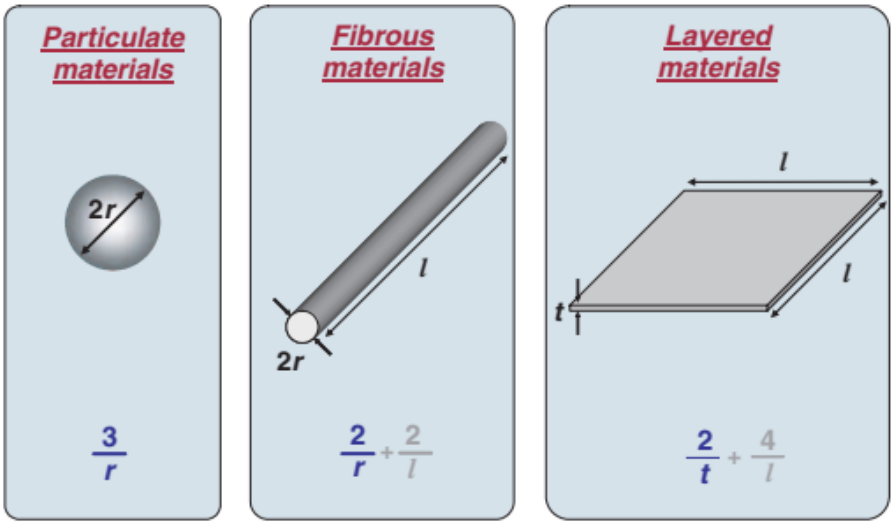


**Figure 2.** Commonly used reinforcements in polymer nanocomposites and their surface area/volume relations. Reprinted from [12] with permission.

Some studies have used carbon nanotubes (CNTs), a fibrous material (Figure 2b), as a filler to shed light on the damping and interface properties of the polymer/CNT nanocomposites. Shur et al., for example, added single-wall carbon nanotubes (SWCNTs) to the polycarbonate (PC) matrix and showed that the failure of the PC/SWCNT interface results in sliding CNTs on the PC matrix and energy dissipation via friction [13]. By adding 1% of CNTs, Gardea et al. doubled the damping of the CNT/polystyrene nanocomposites, in which CNTs were aligned in the direction of axial stress as seen in Figure 3 [14]. Additionally, Ashraf et al. studied the effect of CNT alignment in the CNT/polystyrene nanocomposites on damping. The highest damping result was obtained from the aligned CNT to the stress direction compared to the off-axis directions. This study showed that as the misalignment angle increases, damping capacity decreases. It also revealed a significant contribution of the interactions between CNTs and the intensified stress fields at locations of CNT-CNT overlap on damping [15]. The same adverse effect of misalignment can be also observed for traditional carbon fiber reinforced polymers [16].

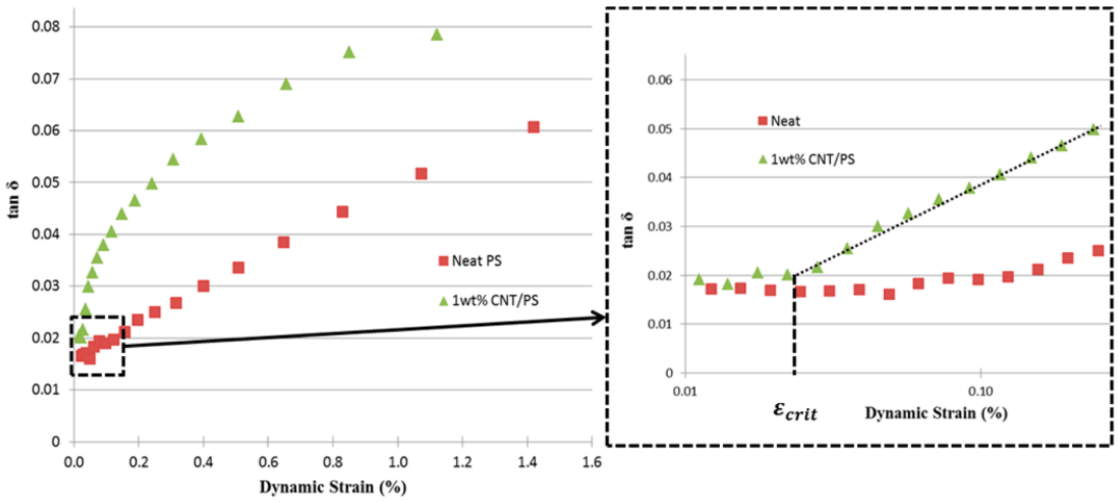


**Figure 3.** Damping results of pure PS and CNT reinforced PS nanocomposites as a function of strain. Reprinted from [14] with permission.

## 2.2. Graphene as a Nanofiller

After the first stable isolation, graphene captured researchers' attention because of its superior mechanical, electric and thermal properties [17,18]. Graphene has the potential to be utilized in almost all applications from energy storage to medical devices due to the combination of the features that no known material has [19,20]. Graphene sheets have theoretically one atom thickness and consist of $sp^2$-bonded carbon atoms [21]. Graphene's carbon atoms are bonded via σ bonds and create honeycomb lattice. This lattice and bonding structure allow graphene to show superior properties [22].

There are currently three main graphene production methods; mechanical exfoliation, chemical exfoliation and chemical vapor deposition (CVD). Exfoliation methods are called "top-down" and cut down the number of the graphene layer in graphite. CVD is called "bottom-up" and grows graphene on a metallic substrate [23]. Mechanical

exfoliation is the first method to obtain graphene, which is also known as the scotch tape method. Although it is a simple peeling process of graphite layer, it is limited by low production volume [17]. Chemical exfoliation method fabricates graphene layer using acids which penetrates and oxidize graphite layers. Oxidized layers separate each other and graphite can be decreased to only 4-5 graphene layers over time [18]. CVD is the most popular graphene production method and it is suitable for large-scale production. This method includes higher vacuum ($10^{-3}$), temperature (below 1000 ºC) and hydrocarbon gas. Carbon atoms attack to the metal substrate and are deposited on the substrate as graphene layers. High-quality graphenes can be yield since the production process can be controlled by temperature and cooling rate [17,24].

### 2.3. Graphene Reinforced Polymer Nanocomposites

Not only CNT but also graphene — another type of carbon-based nanofiller which can be obtained from natural sources by exfoliating graphite [23,25] — could be a good source of damping because of the large interfacial area between the constituents for frictional sliding.

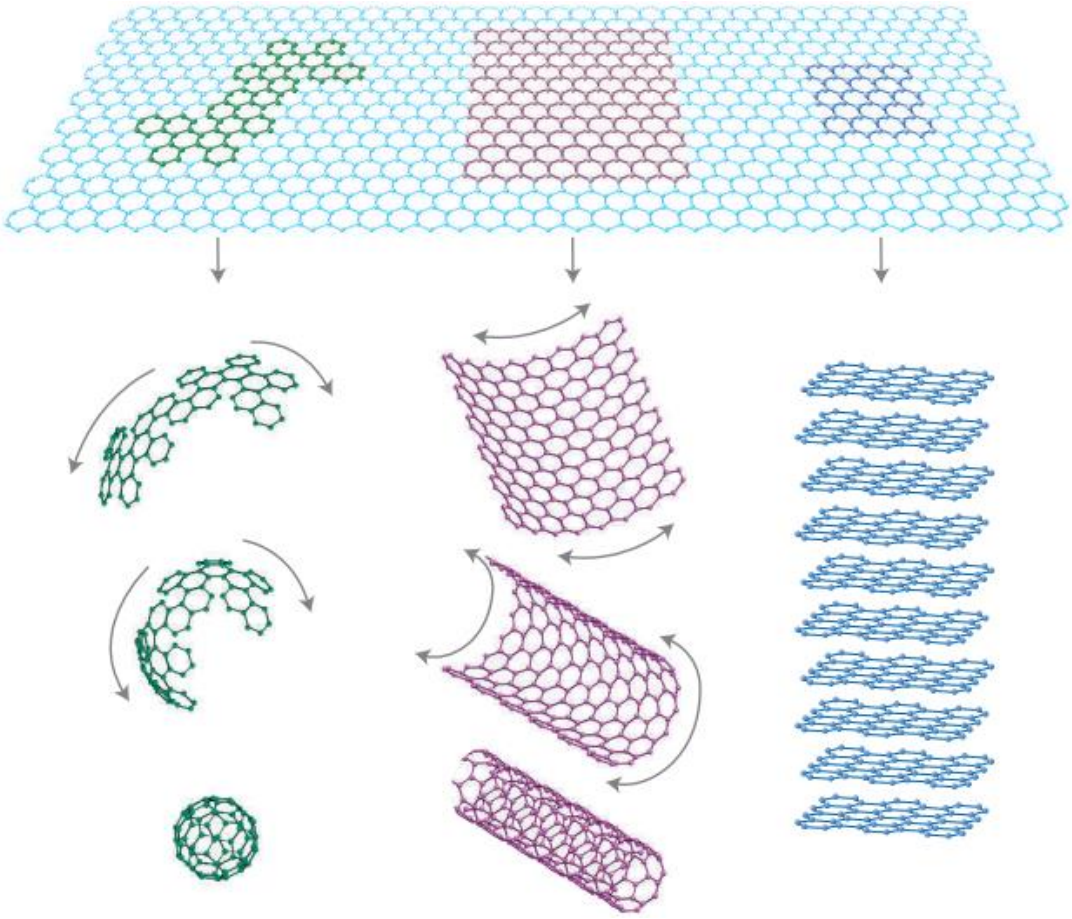

**Figure 4.** 2D structure of graphene might be seen as a source of all carbon-based fillers. Reprinted from [26] with permission.

Although both CNTs and graphene have the ability to improve the properties of materials, a fundamental question about using graphene for damping has remained unclear: *Which one is able to provide higher increments in damping, CNTs with their tubular structure or graphene nanoparticles composed of very similar atoms and atomic bonds but with a stacked sheet-like structure?* There are some studies suggesting that that graphene is more effective than CNT as a filler as it may provide more efficient load

transfer [18,27]. For instance, Rafie et al. have reported a 30% increase in tensile strength of nanocomposites by adding 0.1% graphene, whereas the addition of the same amount of CNTs increased the strength by only 3% [28]. Also, a Raman stereoscopy study has shown a great stress transfer to graphene flake in graphene/polymer nanocomposites, likely facilitated by the large free surfaces of the graphene [29]. Moreover, the energy dissipation in polymer nanocomposites is mainly due to frictional sliding between nanofillers and polymer matrix, often referred to as stick-slip or slippage mechanism. The large surface area of nanofillers along which they interact with polymer chains can be a significant source of increased damping properties [30,31]. Graphene has the potential to be a decent candidate for intrinsic damping applications since the 2D planar structure of graphene can lead to different morphologies inside the matrix than CNT, which has a much higher lateral stiffness due to its tubular structure. These morphological differences could affect the load transfer and matrix-filler slippage, and correspondingly, the damping properties.

In addition, recent temperature-sweep DMA tests proved that graphene can boost damping and increases glass transition temperature ($T_g$) due to the reduction of chain mobility [32–34]. Although temperature-sweep DMA is an excellent test method to determine $T_g$ by utilizing damping properties, it does not provide information about energy dissipation and interface failure. Moreover, the temperature-sweep test represents a single strain state before, during, or after the interface has been destroyed. By using a strain-sweep test one can distinguish the pre and post sliding behavior. The strain-sweep testing would be more appropriate than the temperature-sweep testing for the damping properties of polymers for structural applications. Besides, strain sweep experiments can be used to

distinguish between pre- and post-sliding energy dissipation. To the best of the author' knowledge, strain-controlled damping study on graphene nanocomposites is missing.

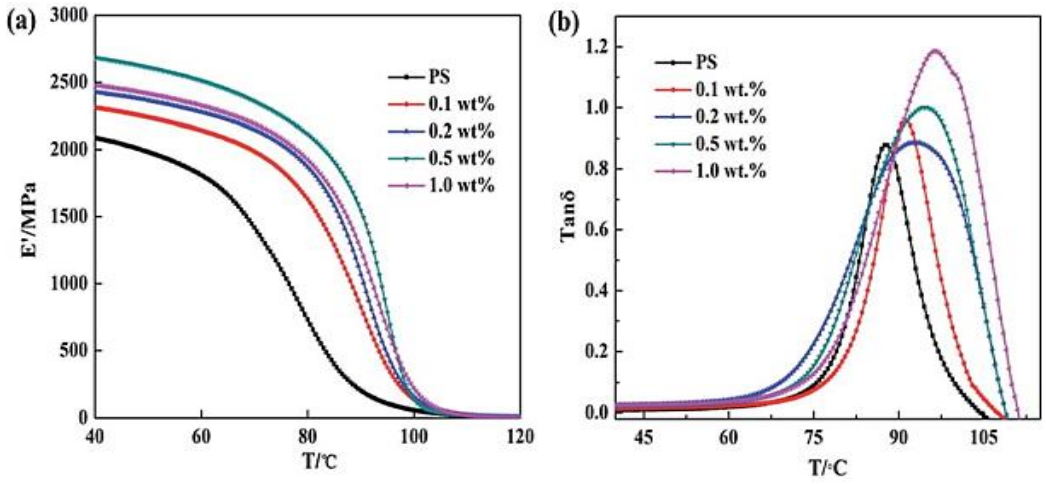


**Figure 5.** a) Storage modulus and b) damping (tanδ) values of functionalized graphene reinforced polystyrene nanocomposites as a function of temperature. Reprinted from [32] with permission.

There are three main processing methods of graphene-polymer nanocomposites. Melt-mixing in which polymer is heated over its glass transition temperature is the easiest and solvent-free process. Nanofillers are dispersed by shear forces in the glassy or molten state [22]. Although the melt-mixing method is the industry's favorite, it promises the worst dispersion properties compared to other fabrication methods [35]. Solution-mixing includes a solvent which usually exfoliates nanofillers and disperses polymer matrix. After blending of filler and polymer in a solvent with the help of a mixing method such as ultrasonication, the solvent is evaporated and polymer nanocomposite is obtained.

Solution mixing usually offers better dispersion and mechanical properties than melt-mixing [36]. Since polymerization of monomers occurs in between nanofiller sheets, it is expected that the in-situ polymerization technique could result in better dispersion and properties [37]. However, a limiting factor is monomers can attach to filler surface and limit chain length and interconnected polymer network. There main dispersion structure which can be observed in polymer nanocomposites by those methods are shown in Figure 6. The most desired structure is exfoliated in Figure 6 (c) but it is hard to fabricate the structure due to the high surface energy of nanofillers and the tendency to agglomerate. Nanofiller functionalization techniques can be employed to increase dispersion, better attachment to a matrix and higher interface strength [38].

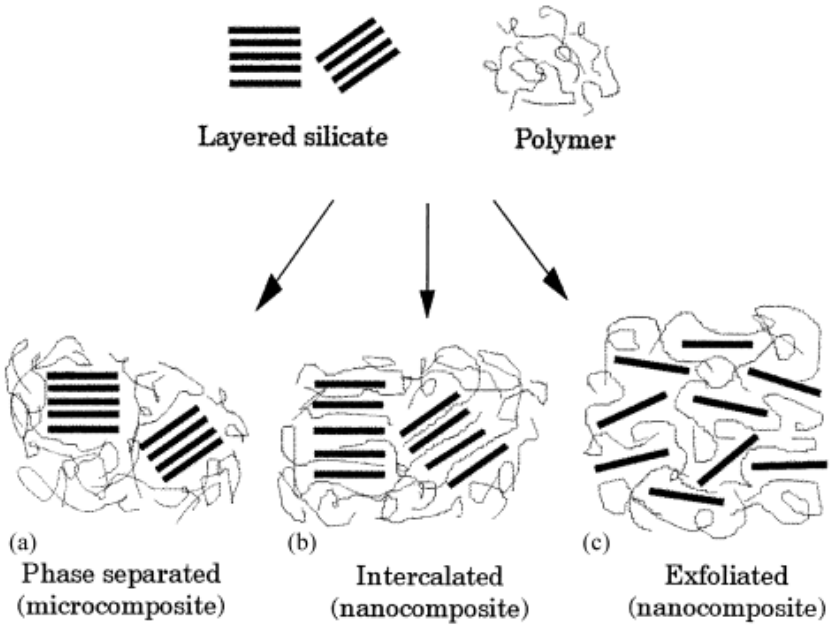


**Figure 6.** Three main dispersion behaviors occurring in nanofiller reinforced polymer nanocomposites. Reprinted from [39] with permission.

In this work, the damping properties of graphene reinforced polymer nanocomposites were investigated through a combined experimental and modeling effort. The graphene nanocomposites were fabricated by using a solution mixing method, and the effects of two graphene types with different surface morphologies and dynamic strain were systematically studied. The different graphenes enabled us to study the aspect ratio and morphology effects on damping. Damping, the ratio of loss and storage modulus, was utilized to compare properties of the neat polymer and polymer/graphene nanocomposites. To develop a better understanding of the damping and slippage mechanism, a micromechanical model was developed.

# 3. EXPERIMENT AND MODEL DESIGN

## 3.1. Fabrication of Graphene Nanocomposites

The fabrication process of graphene reinforced polystyrene nanocomposites is schematically shown in Figure 7. Single layer graphene (SLG) and graphene nanoplatelets (GNP) were purchased from ACS Materials and used as is to compare the effects of aspect ratio and graphene morphology on damping of nanocomposites. The thickness of as-received SLG and GNP were 0.6-1.2 nm and 1-2 nm, respectively. The lateral sizes of SLG and GNP are 0.4-5 μm and 5-10 μm, respectively. As a matrix material, polystyrene (PS) was purchased from Sigma-Aldrich Co. In order to fabricate the composites, a solution mixing process was selected with dimethylformamide (DMF) as a solvent to disperse GNP and SLG in the polymer matrix. The nanoparticle/matrix weight ratio was chosen as 1% for all samples. In the first step, PS and GNP were dissolved in DMF separately, and the mixtures were sonicated for 30 minutes via Pro Scientific VCX-750 13 mm tip sonicator. After the dispersion, two mixtures were blended and sonicated for an extra 15 minutes. To evaporate DMF, the solution was taken onto a hot plate for 20 minutes at 200 ºC, and it was mechanically stirred via a magnetic stir bar at 150 rpm. To dispose of the residue solvent, it was dried in a vacuum oven for 12 hours at 80 ºC. To eliminate voids resulting from the solvent evaporation and drying processes, the sample was mixed via twin-screw microexturder at 100 rpm for 30 minutes. The extrusion process was carried out at 150 ºC. Then, the sample was hot pressed to form the desired shape and

is referred to as PS/GNP, hereafter. To fabricate SLG reinforced PS nanocomposites the same steps were applied, and the samples were labeled as PS/SLG.

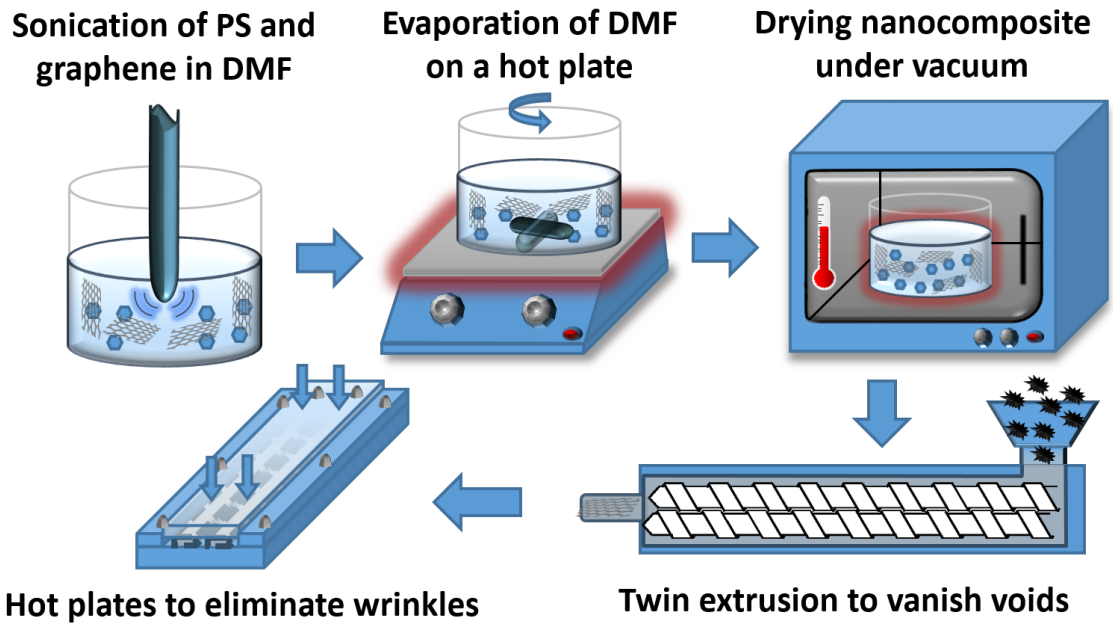


**Figure 7.** The schematic demonstration of the production of GNP/PS and SLG/PS nanocomposites via a solution mixing process.

### 3.2. Mechanical and Material Characterization of Graphene Nanocomposites

Dynamic mechanical analysis (DMA) tests were conducted via TA Instruments DMA Q800. The dynamic loads, tension and compression, were applied parallel to the extrusion direction. The strain amplitude was between 0-0.3% with a zero offset strain. The test frequency was set to 1 Hz and all DMA tests were conducted at room temperature. The strain magnitude applied were selected based on the values that air vehicles

experience [40]. To calculate optimum gage length and sample thickness $\varepsilon = \pi^2/3 * (t/L)^2$ was used to avoid buckling. The approximate required buckling force was calcuated as 27 N which is below the load cell limit of 18N. Five PS/GNP and PS/SLG DMA test samples were approximately 0.6 mm thick, 2 mm wide and 20 mm long with 10 cm gauge length. Scanning electron microscope (SEM) images of GNP and SLG were taken via Tescan LYRA-3. SEM images of the samples were taken from fracture surfaces that were parallel and perpendicular to the extrusion direction.

### 3.3. Micromechanical Model of Damping Characterization

In order to estimate the damping behaviors of the graphene reinforced polymer nanocomposites, a model, which was previously used to interpret and calculate the damping behaviors of CNT reinforced polymer composites, was utilized [14,40]. The model is based on the shear-lag theory by Cox in 1952 [41] and has proven to be reliable in comparison with graphene/polymer interface experiments [29,42]. Damping estimation model was modified based on graphene's intrinsic geometric and morphological properties.

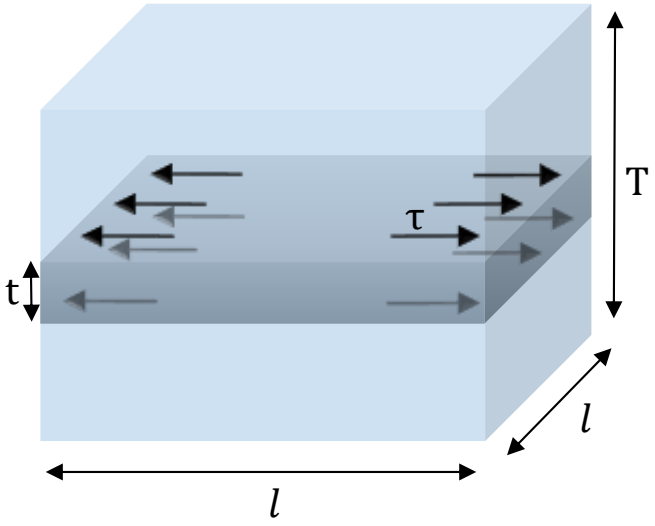


**Figure 8.** Representative Volume Element (RVE) of a graphene flake embedded in a polymer matrix.

The representative volume element (RVE) can be seen in Figure 8 where the graphene flake is surrounded by the polymer matrix. It is important to mention that this model assumes that the only source of damping except for the viscoelastic behavior of the polymer matrix is the friction between nanofiller and matrix. Thus, in the model, no friction and frictional damping behavior are expected until the applied dynamic strain amplitude reaches the values required for partial sliding along with the interface. In this pre-slip regime, the interfacial shear stress ($\tau$) can be calculated by Eq. 1 [29].

$$\tau(x) = E_G \varepsilon_m n \left[\frac{sinh(nx/t)}{cosh(nl/2t)}\right], \text{ where } n = \sqrt{\frac{2G_m}{E_G}\left(\frac{t}{T}\right)} \quad (1)$$

where $E_G$ is graphene modulus, $\varepsilon_m$ is the stress applied to the matrix, $l$ and $t$ are the graphene length and thickness, respectively. $T$ is the thickness of the RVE, which is

determined by using the volume fraction of graphene from the experiment and $G_m$ is the shear modulus of the matrix. The variable $x$ represents a point on a graphene flake bound to $\pm\, l/2$ with the graphene midpoint chosen as the origin.

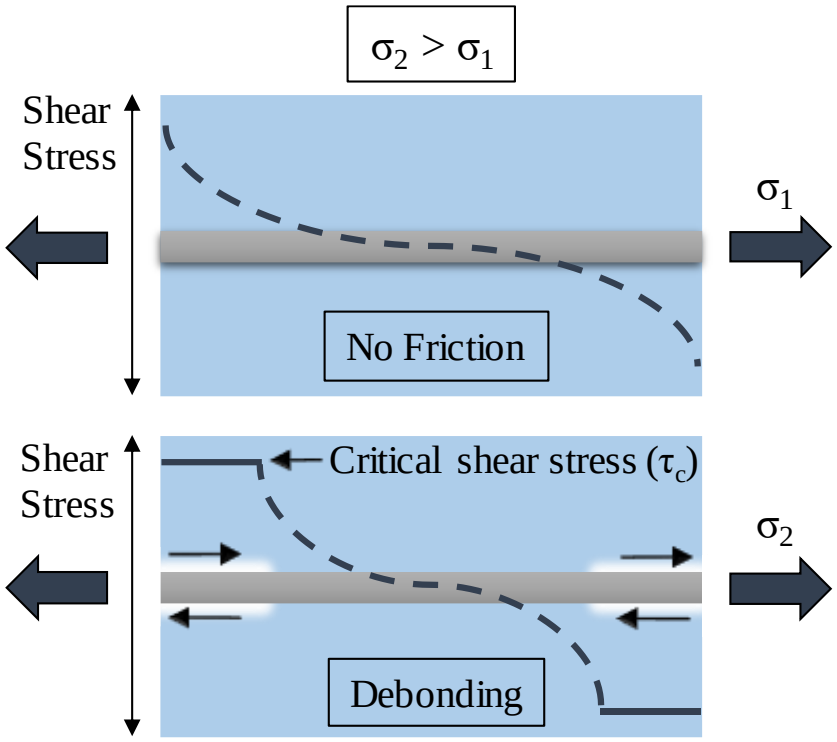


**Figure 9.** Schematic demonstration of how debonding and friction occur in polymer nanocomposites.

Once shear stress reaches the critical value ($\tau_{cr}$), the stick-slip mechanism is activated and the graphene-polymer interface is partially debonded depending on the

applied strain rate. Therefore, the damping mechanism which results from the interfacial friction starts. In this model, as the interface fails, the debonded parts of graphene flakes can only transfer the load to the matrix via friction with a constant shear stress of $\tau_{cr}$. For this reason, it is assumed that interfacial shear stress ($\tau$) remains constant after the failure occurs [43]. This slippage mechanism is shown in Figure 9**.**

In this model, the maximum shear stress occurs at the edges of flakes. By setting $\tau(x) = \tau_{cr}$ in Eq. 1., the required critical strain ($\varepsilon_{cr}$) to initiate the stick-slip mechanism can be obtained in Eq. 2.

$$\varepsilon_{cr} = \frac{\tau_{cr}}{nE_G \tanh(nl/2t)} \tag{2}$$

At strains of $\varepsilon_{xx}$ higher than $\varepsilon_{cr}$, the length over which slip occurs ($l'$) can be calculated by solving Eq. 1. for x when $\tau(x) = \tau_{cr}$:

$$\frac{l'}{2} = \frac{l}{2} - \frac{t}{n} Arcsinh\left(\frac{\tau_{cr}\cosh(nl/2t)}{\varepsilon_{xx}E_G n}\right) \tag{3}$$

The dissipated energy due to the friction can be calculated via Eq. 4. The stored energy is obtained by Eq.5. where $\overline{K}$ is the stiffness of the composite. $\overline{K}$ values were collected from the experimental results for model accuracy. The $\varepsilon_{xx}$ is the applied dynamic strain amplitude. Damping ($tan\delta$) is then calculated as the ratio of dissipated energy ($\delta U$) to the stored (Elastic) energy ($2\pi U_0$) and can be obtained in Eq. 6. The model parameters and their relations to the experiments are presented in Table 1**.**

$$\delta U = 2\int_{\varepsilon'}^{\varepsilon_{max}} f(\varepsilon_{xx})\frac{l'(\varepsilon_{xx})}{2}d\varepsilon_{xx} \tag{4}$$

$$2\pi U_0 = \pi\bar{K}(\varepsilon_w l/2)^2 \tag{5}$$

$$tan\delta = \eta = \frac{\delta U}{2\pi U_0} \tag{6}$$

# 4. RESULTS AND DISCUSSION

## 4.1. Morphological Insight of Graphene and Graphene Nanocomposites

The viscoelastic responses of PS and PS matrix nanocomposites with two types of fillers, GNP and SLG, were studied. The two fillers have very distinct morphologies. The GNP is mostly flat while the SLGs have a wrinkled geometry. The SEM images of GNP, SLG, and nanocomposites are first presented, followed by the PS/GNP and PS/SLG nanocomposites, respectively.

Figure 10 (a) and (b) present the SEM images of the as-received GNPs and SLGs to provide the morphological and dimensional difference between two graphene types. According to their technical data sheets, their chemical compositions are almost identical with high carbon and very low oxygen ratio [44]. The GNP flakes in Figure 10 (a) are wide open and look relatively discrete. On the other hand, SLGs tend to cluster and look like cotton flowers, as seen in Figure 10 (b). Another marked distinction between the fillers is that GNP has a higher lateral size promising higher filler/matrix friction area.

The cross-section SEM images of PS/GNP and PS/SLG nanocomposite are demonstrated in Figure 11 (c) and (d). The images were taken along the extrusion and stress direction. In Figure 11 (c), GNP flakes align parallel to the extrusion direction due to the extrusion process. This is likely because of the larger size of the GNP particles, as a result, they will experience larger shear forces by the matrix during extrusion. The particles are quite flat and the surfaces are smooth without any visible wrinkles in the SEM resolution level. However, in Figure 11 (d), SLGs are wrinkled and look considerably

smaller in terms of length and lateral size in a comparison with GNPs. There is no visible alignment in the extrusion direction. Unlike GNP, the extrusion process has no noticeable effect on alignment and flattening of the SLGs. The cumulative amount of the lateral surfaces which is parallel to the applied stress is higher in PS/GNP than PS/SLG.

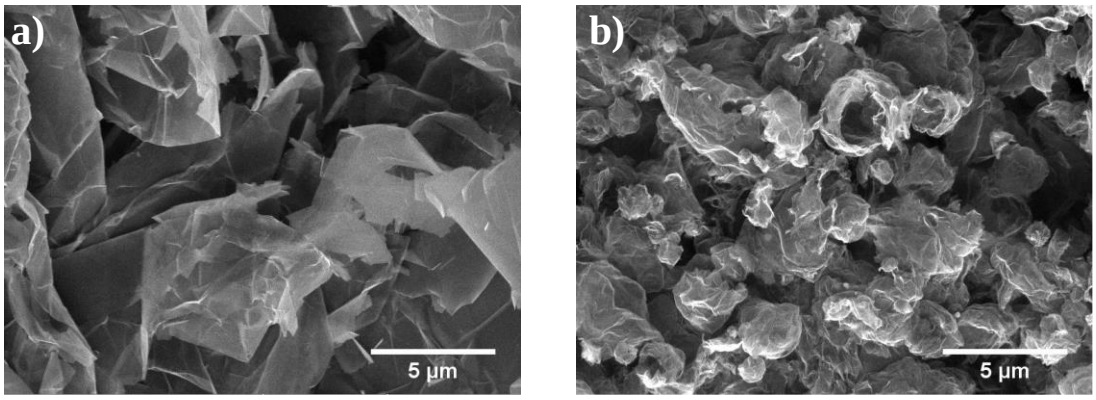


**Figure 10.** The SEM images of a) as received GNP, b) as received SLG

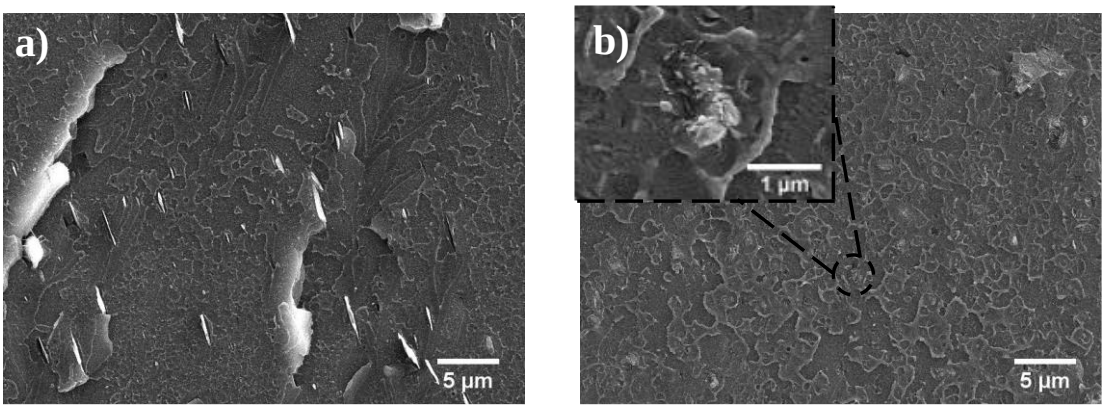


**Figure 11.** The SEM images of the cross-section of a) PS/GNP and b) PS/SLG nanocomposites perpendicular to the extrusion direction. Images are taken from fracture surfaces perpendicular to the extrusion direction.

### 4.2. Damping Ratio and Storage Modulus of PS/GNP

Figure 12 and Figure 13 illustrate the storage modulus and damping ratios of PS and PS/GNP as a function of dynamic strain with error bars which represent the experimental uncertainty. In Figure 12, the mechanical reinforcing effect of the GNP is evident, especially at the lowest applied dynamic strain amplitude. The storage modulus of PS and PS/GNP at low strains are respectively 2.77 ±0.086 GPa and 2.91 ±0.092 GPa. However, the storage modulus of PS/GNP drops nearly twice as fast with the dynamic strain amplitude compared to the neat PS. At 0.3% dynamic strain, the storage modulus of PS/GNP becomes smaller than pure PS. Thus, PS/GNP samples have damage accumulation mechanisms which are not present in PS. These additional damage mechanisms can only exist in certain regions within the nanocomposite such as PS – GNP and GNP – GNP interface.

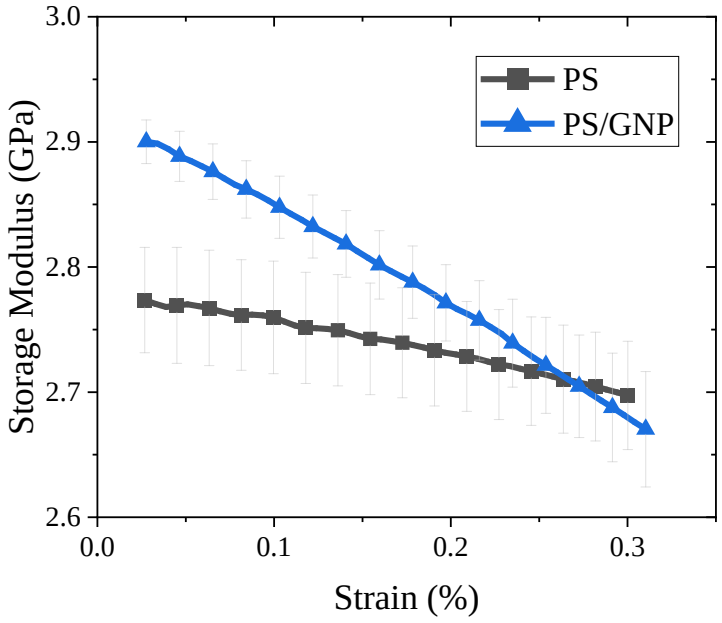


**Figure 12.** The experimental DMA results of the storage modulus of neat PS and PS/GNP nanocomposite with a function of dynamic strain

More insight into the nature of these damage mechanisms that are peculiar to the PS/GNP can be obtained from the damping response of the material, as seen in Figure 13. It is interesting to note that the drop in the storage modulus of PS/GNP, in comparison to the neat PS, coincides with a considerable increase in damping. To compare the damping increments of PS and PS/GNP, the slopes were calculated by using a curve fitting tool. It was found that the damping increase rate of PS/GNP doubles the rate of pure PS. This damping behavior is in line with a progressive partial debonding along with interfaces in the nanocomposite, in which the interface can carry load via frictional sliding. Frictional sliding can occur between PS and GNP, similar to the PS-CNT interfaces [14,15], or between the graphene layers within each GNP particle. The latter is a likely mechanism

in nanocomposites that are reinforced with GNP since graphene-graphene interfaces are generally weaker than graphene-polymer interfaces [45,46].

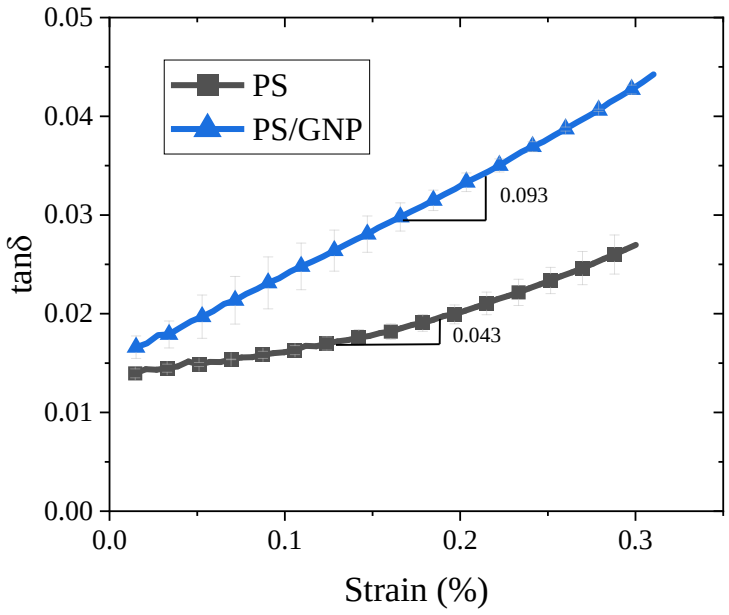


**Figure 13.** The experimental DMA results of a) tanδ of neat PS and PS/GNP nanocomposite with a function of dynamic strain

Moreover, unlike the CNTs in CNT-reinforced nanocomposites in which only the outer shells of CNTs are accessible to the matrix, the matrix can apply shear forces to graphene flakes, causing the graphene within a graphene flake to slide on each other further dissipating energy. Indirect evidence in support of the graphene-graphene sliding even prior to PS-GNP sliding is the difference between the damping behavior in GNP/PS and CNT/PS [14,15]. While in CNT/PS in Figure 14, the damping ratio shows a plateau

at small strains prior to the onset of interfacial slippage [47], in GNP/PS, the damping increases with the applied strain even at the lowest strain applied. Thus, it can be deduced that the energy dissipation mechanism is already activated in PS/GNP in very low strain range. In addition, the tanδ slope of PS/GNP samples is almost six times higher than CNT counterparts having the same weight filler ratio. Even the slope of 2 wt% PS/CNT is lower than PS/GNP having 1% filler ratio.

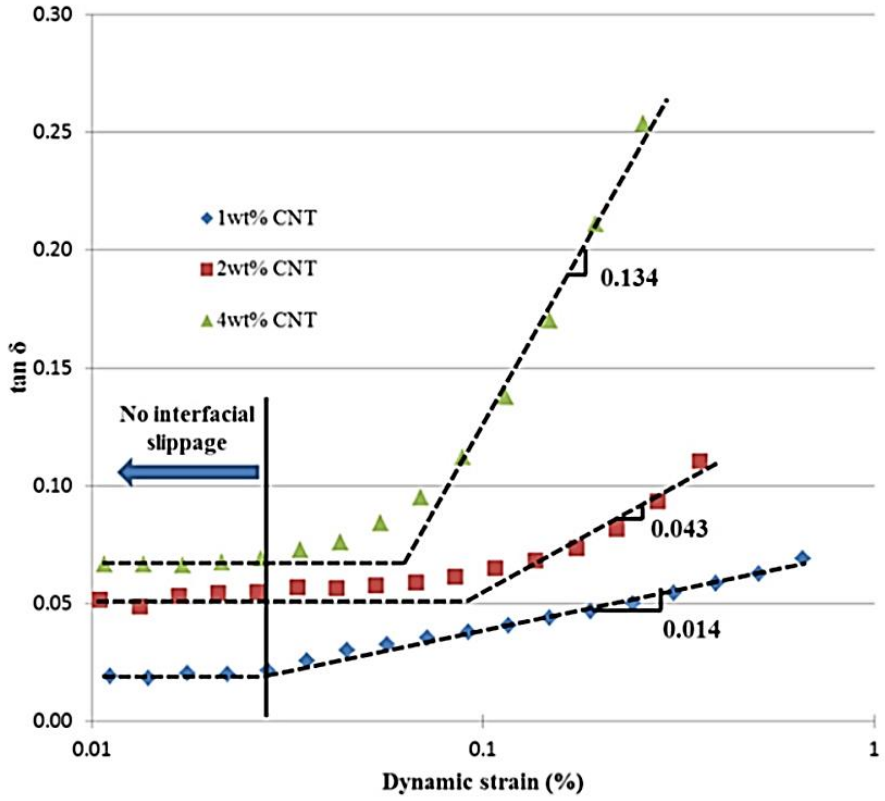


**Figure 14.** Damping of PS/CNT nanocomposites for different CNT weight percentages. In the low strain regime, there is no slippage filler/polymer slippage, which is not a case in the graphene/polymer system. Reprinted from [47] with permission.

### 4.3. Comparison of Micromechanical Model and Experimental Results

The experimental results presented so far demonstrate the effect of GNPs on damping of nanocomposites. However, no direct information can be obtained about the stress fields around GNPs through the experiments. Thus, the shear-lag model was used to develop a deeper insight into the damping behavior of the graphene reinforced polymer nanocomposites. The model relates the damping behavior in nanocomposites to matrix-filler interface partial debonding and frictional sliding between them. Other damping mechanisms such as matrix tearing, stress concentrations and the friction between the graphene layers are not considered in this model. The essential components of the model are obtained based on our earlier work [14], and the details of the model are explained in the section of the Micromechanical Model of Damping Characterization.

**Table 1.** Input data for the micromechanical damping model

| **Model parameter** | **Value used** | **Relation to experiment** |
|---|---|---|
| GNP Concentration | 1 wt. % | Fabrication |
| Aspect Ratio (A.R) | 5000 | Manufacturer and SEM images |
| Average GNP length | 5 μm | SEM images |
| Thickness | 1 nm | Manufacturer and [48] |
| Critical Strain | ~0.035 % | Eq. 2 |
| Interfacial Shear Strength | 0.50 MPa | [14] |
| GNP elastic modulus | 300 GPa | Fitting parameter, within the range of experimental measurements [49] |
| Modulus of the matrix | 2.25 GPa | Tensile Test |

The inputs of the model are summarized in Table 1. The thickness of single layer GNP was chosen as 1 nm based upon the previous experimental studies [48]. The length of GNPs used in the model were the average values from SEM images, 5 μm, which is in the range of the technical data sheet provided by the manufacturer. The modulus of the matrix was determined via a simple tensile test as 2.25 GPa. The model takes the post-interface debonding interfacial shear stress as the input to calculate the value of the damping coefficient. This value can be obtained from literature in the range of ~0.3-2.3 MPa [23,29,42,50]. However, this value highly depends on the surface chemistry, morphology and length of graphene [51]. For our experiments carried out on GNP/PS systems, a value of 0.50 MPa, which was previously reported for the CNT/PS system [14], was chosen due to similarities between the surface chemistry of CNTs and GNP as well as their similar surface topography (smooth surfaces in both cases).

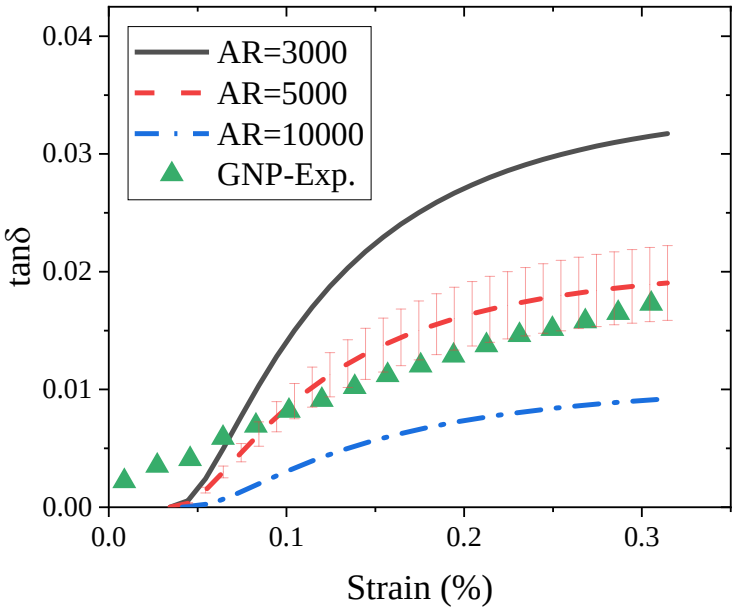


**Figure 15.** The comparisons of the model and experimental damping (tanδ) values.

The predictions of the model at low strains (below ~0.1%) are not in line with the experimental data. A likely cause for the experiment-model difference in the low strain regime is the graphene-graphene sliding and friction which is not considered in the model [52,53]. Quantitatively, the effective graphene interlayer strength, especially for smooth GNPs shown in Figure 10 (a), can be as low as 0.02 MPa, which is two orders of magnitude smaller than the polymer-graphene interface due to the low van der Waals (vdW) force interactions [45]. Thus, graphene sheets within GNPs can dissipate energy by sliding over each other even in very low strain regime [46,54]. GNP-GNP sliding presents an important distinction between vibration damping in GNP-reinforced and CNT-reinforced nanocomposites, as discussed earlier in this section. In PS/GNP, the axial

loading of the matrix can induce shear stresses on GNP by sliding the two surfaces of GNP in opposite directions. The main load transfer mechanism between the two surfaces is the vdW interactions, allowing for mutual sliding and energy dissipation between the surfaces. This is unlike CNT/PS composites in which only the CNTs outmost shell is in contact with the matrix. However, the graphene-graphene sliding can only be fully active at very small strains mainly because of the constraints imposed on the GNPs by the PS. The mechanical constraints imposed on the edges of GNP sheets can suppress the sliding between graphene sheets within a GNP particle allowing for other damping mechanisms such as the PS-GNP interfacial sliding to manifest itself.

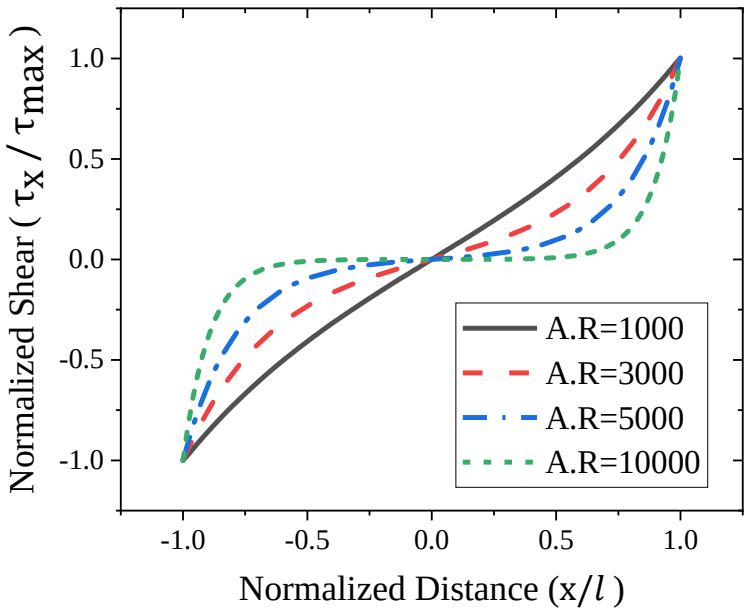


**Figure 16.** The distribution of the interfacial shear stress on a graphene flake as a function of the graphene aspect ratios. The shear stress and distance are normalized by an applied stress and graphene length, respectively. The applied strain is 0.3%.

The model allows us also to consider hypothetical cases and predict the damping of PS/GNP with different aspect ratio values compared to tested experimentally. For instance, Figure 15 illustrates that lower aspect ratios increase the damping of graphene nanocomposites. The GNP having an aspect ratio of 3000 has higher damping than the aspect ratios of 5000 and 10000. This behavior roots in the dependence of the shear stress distribution on filler aspect ratio values. As shown in Figure 16, the shear stress distribution is more uniform and quasi-linear when the aspect ratio is rather low enough (A.R. = 3000 and 1000). Thus, shorter graphenes experience higher interfacial shear stress and interfacial debonding. On the other hand, when the aspect ratio is increased, the shear stress is concentrated on the edges of the graphene, and the middle parts of the graphene expose to lower shear stress, which reduces the debonded length for any given dynamic strain amplitude.

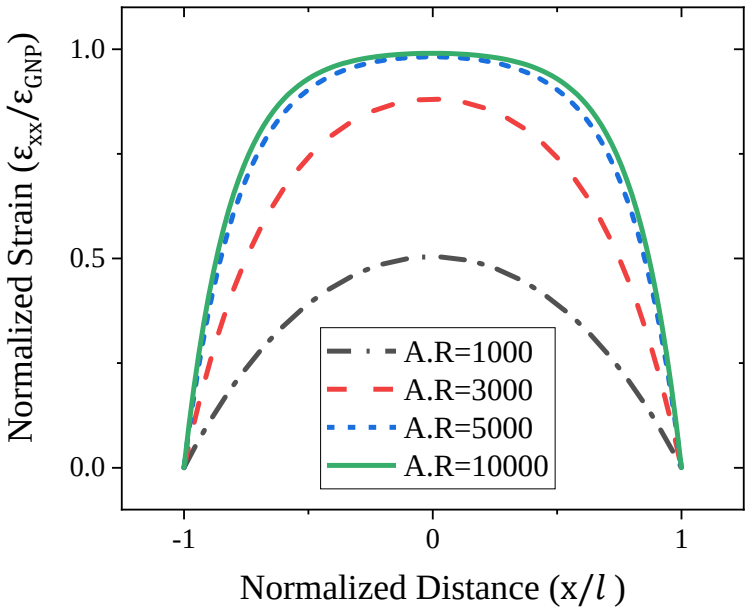


**Figure 17.** The distribution of the strain on a graphene flake as a function of the graphene aspect ratios. Strain and distance are normalized by an applied strain and graphene length, respectively. The applied strain is 0.3%.

Although lower aspect ratio graphene increases damping, they reinforce less effectively. As shown in Figure 17, for relatively small aspect ratios, the strain experienced by the graphene will not reach the far field strain values; thus, the load is only partially carried by the filler. Graphene having 1000 aspect ratio can experience ~50% of the applied strain, while at an aspect ratio of 3000, the strain experienced by the graphene can be ~75% of the applied strain, and for aspect ratios higher than 5000, the strain of the fillers is nearly the same in the matrix and graphene, therefore, higher reinforcement rates can be observed.

### 4.4. Damping Ratio and Storage Modulus of PS/SLG

In order to experimentally validate one of the model predictions, i.e., the relationship between damping and aspect ratio of fillers, damping behavior of polymers which were reinforced with single layer graphene (SLG) were studied. The PS/SLG nanocomposites were fabricated by using the solution mixing method discussed in Fabrication of Graphene Nanocomposites (Ch. 3.1.). PS/SLG was tested via DMA using the same test procedure.

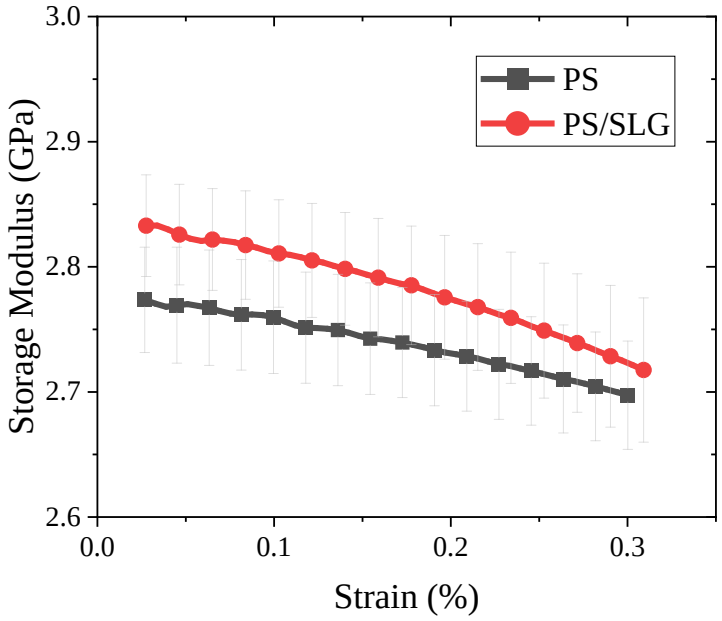


**Figure 18.** The experimental storage modulus of PS/SLG and PS with a function of dynamic strain

The storage modulus of PS/SLG is higher than PS suggesting that SLG provides mechanical reinforcement as seen in Figure 18. However, SLGs provide less reinforcement rate and load transfer efficiency as the model suggests. Adding 1% of GNP increases storage modulus by ~0.13 GPa whereas adding the same amount of SLG increases only by ~0.06 GPa. Moreover, the slopes of the PS and PS/SLG are nearly the same up to the dynamic strain amplitude of 0.2%, suggesting no damage accumulation or significant interfacial sliding between SLGs and the matrix. In addition, as shown in Figure 19, the damping ratio of PS/SLG is almost identical to pure PS's ratio until 0.2% strain. Using this value of strain as the critical strain threshold for interfacial sliding, the shear strength of the PS-SLG interface was calculated from Eq.2. The $\tau_{cr}$ is calculated to be ~7.5 MPa for PS/SLG, which is one order of magnitude higher than PS/GNP. On the other hand, once the applied strain reaches ~0.2%, the modulus of PS/SLG starts to drop at a slightly higher rate than the PS. The drop in modulus coincides with a slight increase in damping of PS/SLG from the value corresponding to the neat PS. At 0.3% strain, adding 1% wt. of SLG to PS increased the tanδ only ~10% although the same amount of GNP raised the ratio by ~70% compared to pure PS. It is emphasized that the drop in modulus and an increase in damping in SLG/PS is much less pronounced than those observed in PS/GNP.

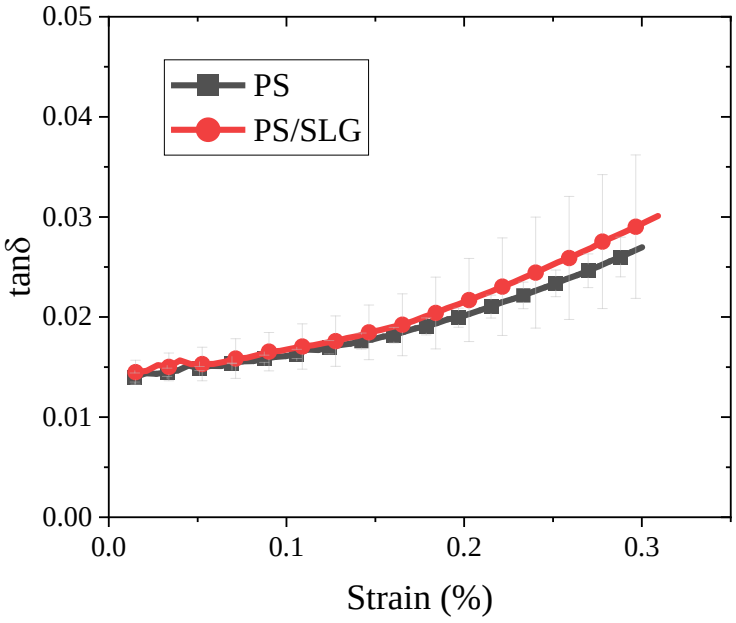


**Figure 19.** The experimental tanδ values of PS/SLG and PS with a function of dynamic strain

### 4.5. The Effect of Graphene Morphology on Damping

Even though the model suggests that a smaller aspect ratio would ensure a higher damping property, the experimental results of PS/SLG oppose this argument. In order to address this discrepancy, we studied the SEM images of PS/GNP and PS/SLG, seen in Figure 10 and Figure 11. The SEM images revealed that GNP has a considerably smoother and flatter surface providing easier sliding on the matrix. Previous research showed that reduced surface roughness of graphene facilitates easier interfacial sliding [55–57]. Therefore, it can be hypothesized that the surface roughness of the SLG, a result of their low bending stiffness, increases the effective interfacial shear strength of the PS/SLG

interface and postpone interfacial sliding to higher strains. This hypothesis is in line with the effective $\tau_{cr}$ of the PS/SLG interface which was calculated earlier in this section to be ~7.5 MPa, compared to a value of less than 1 MPa for the PS/GNP interface.

The force applied is directly transferred to the GNP interface while it is transferred to the SLG surface with various angles, which decreases the amount of force affecting PS/SLG interface. These two morphological mechanisms imply the GNP slippage on the polymer surface is more feasible than SLG slippage. The SEM images of GNP and SLG are illustrated to demonstrate how an applied force effects the graphene/polymer interface in Figure 20. In PS/GNP nanocomposites, since GNPs are flat and parallel to the stress direction, the applied force directly affects the interface as a shear force. Therefore, it entirely contributes to the graphene slippage, which is shown in Figure 20 (a). However, the applied force to the PS/SLG interface is diverted into two different stresses as either tension or compression and shear. Due to its waviness structure, the force magnitude is shared by the tension or compression and shear stresses and mechanical interlocking occurs. Therefore, the magnitude of shear stress, which causes the filler slippage and damping, becomes smaller and the interface experiences less stress. Consequently, the debonding mechanism in PS/SLG is delayed and less effective for damping, in a comparison with PS/GNP.

A careful study of the SEM images revealed another factor, alignment of fillers, which can result in considerable differences between the damping behavior of PS/GNP and SLG/PS. As seen in Figure 11, SLGs are randomly oriented in the matrix while GNPs are aligned in the direction of the extrusion. GNP/PS is expected to have higher damping

ratio since off-aligned fillers experience less interfacial shear stress [58] and show reduced loss modulus and damping ratio [15].

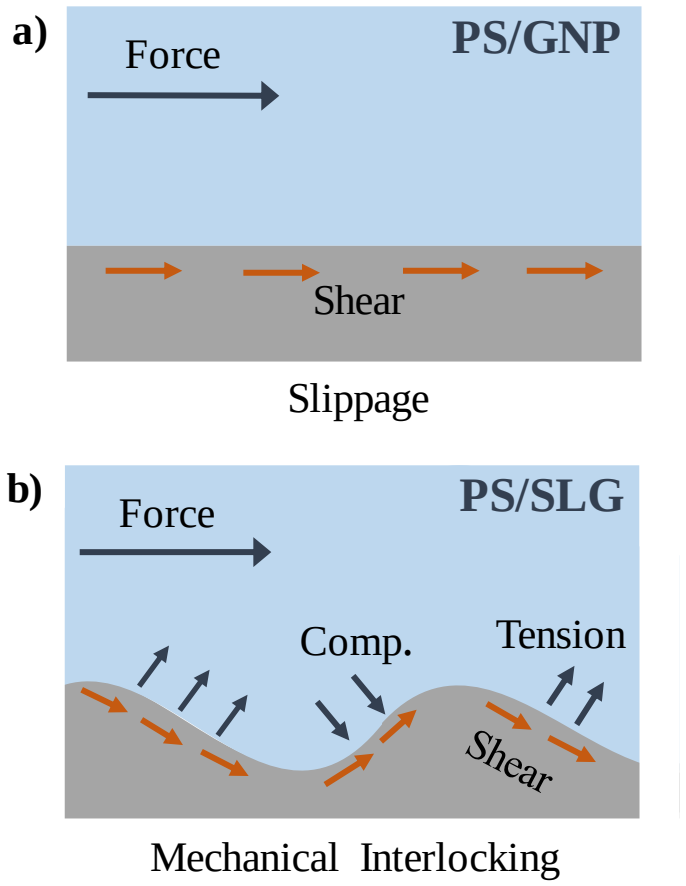


**Figure 20.** The schematic illustration of the forces influencing the a) PS-GNP and b) PS-SLG interface

# 5. CONCLUSION AND FUTURE DIRECTIONS

## 5.1. Conclusion

The damping and interface behaviors of graphene reinforced polymer nanocomposites were studied through combined experiments and continuum modeling approach. The experiments consisted of dynamic mechanical loading of PS-graphene samples with dynamic strain amplitudes of 0.3% and less. Two types of graphene nanoparticles with different morphologies and aspect ratios were used as fillers: the so-called single layer graphene (SLG) and graphene nanoparticles (GNP). At the highest dynamic strains tests, PS/GNP nanocomposites showed a ~70% increase in damping properties compared to the neat polymer. This was in contrast to PS/SLG samples in which enhancement in damping was considerably low (~10%). The low damping augmentation in PS/SLG is also in contrast to the predictions of our micromechanical models. To further investigate the origin of discrepancy between model and experiment, the morphology of the nanocomposites was studied in SEM. The experiments revealed that the SLG samples are highly wrinkled in contrast to the rather flat surfaces of GNPs.

The experimental results pointed to a considerable effect of graphene morphology in facilitating (or delaying) the interfacial failure, leading to enhanced (or reduced) damping performance. The combined modeling-experimental work suggests that the wrinkles on the surface of SLG, caused by its low bending stiffness, were a major player in enhancing the interfacial shear strength (IFSS) between the polymer and the graphene, leading to ~15x improvement in IFSS. This result points to a considerable effect of

graphene morphology in facilitating the interfacial failure in GNPs (in contrast to SLG), leading to enhanced damping.

### 5.2. Future Directions

Further studies shall be dedicated to further investigation of interface and damping properties of graphene polymer nanocomposites. The present and previous works have shown that the sliding mechanism of filler on the matrix has a remarkable increase in damping. Critical activation strain of sliding and frictional energy on interface directly affect the damping behaviors. Thus, further studies which are controlling the interface strength via functionalization or oxidation of graphene should be conducted.

Graphene reinforced polymer nanocomposites could be used as a matrix material in traditional carbon fiber composite instead of pure epoxy. The properties of carbon fiber/graphene/polymer nanocomposites should be investigated.

# REFERENCES


[1] I.C. Finegan, R.F. Gibson, Recent research on enhancement of damping in polymer composites, Compos. Struct. 44 (1999) 89–98. doi:10.1016/S0263-8223(98)00073-7.

[2] G.M. Kamath, N.M. Wereley, M.R. Jolly, Characterization of Magnetorheological Helicopter Lag Dampers, J. Am. Helicopter Soc. 44 (1999) 234–248. doi:10.4050/JAHS.44.234.

[3] P.P. Friedmann, D.H. Hodges, Rotary Wing Aeroelasticity-A Historical Perspective, J. Aircr. 40 (2003) 1019–1046. doi:10.2514/2.7216.

[4] B. Panda, E. Mychalowycz, F.J. Tarzanin, Application of passive dampers to modern helicopters, Smart Mater. Struct. 5 (1996) 509–516. doi:10.1088/0964-1726/5/5/001.

[5] D.L. Kunz, Influence of elastomeric damper modeling on the dynamic response of helicopter rotors, AIAA J. 35 (2012) 349–354. doi:10.2514/3.13509.

[6] E.W. Aiken, R.A. Ormiston, L.A. Young, Future Directions in Rotorcraft Technology at Ames Research Center, in: Proc. 56th Am. Helicopter Soc. Annu. Forum, 2000: pp. 1–22.

[7] W. Hu, N.M. Wereley, Hybrid magnetorheological fluid-elastomeric lag dampers for helicopter stability augmentation, Smart Mater. Struct. 17 (2008). doi:10.1088/0964-1726/17/4/045021.

[8] Z. Gong, J. Gong, X. Yan, S. Gao, B. Wang, Investigation of the effects of

temperature and strain on the damping properties of polycarbonate/multiwalled carbon nanotube composites, J. Phys. Chem. C. 115 (2011) 18468–18472. doi:10.1021/jp205354e.

[9] L.M. Corso, D.A. Popelka, M.W. Nixon, Design, Analysis, and Test of a Composite Tailored Tiltrotor Wing, J. Am. Helicopter Soc. 45 (2000) 207. doi:10.4050/JAHS.45.207.

[10] E. SMITH, I. CHOPRA, Aeroelastic response and blade loads of a composite rotor in forwardflight, in: 33rd Struct. Struct. Dyn. Mater. Conf., American Institute of Aeronautics and Astronautics, Reston, Virigina, 1992. doi:10.2514/6.1992-2566.

[11] J. Suhr, N. Koratkar, P. Keblinski, P. Ajayan, Viscoelasticity in carbon nanotube composites, Nat. Mater. 4 (2005) 134–137. doi:10.1038/nmat1293.

[12] E.T. Thostenson, C. Li, T.W. Chou, Nanocomposites in context, Compos. Sci. Technol. 65 (2005) 491–516. doi:10.1016/j.compscitech.2004.11.003.

[13] J. Suhr, N. Koratkar, Energy dissipation in carbon nanotube composites: A review, J. Mater. Sci. 43 (2008) 4370–4382. doi:10.1007/s10853-007-2440-x.

[14] F. Gardea, B. Glaz, J. Riddick, D.C. Lagoudas, M. Naraghi, Energy Dissipation Due to Interfacial Slip in Nanocomposites Reinforced with Aligned Carbon Nanotubes, ACS Appl. Mater. Interfaces. 7 (2015) 9725–9735. doi:10.1021/acsami.5b01459.

[15] T. Ashraf, M. Ranaiefar, S. Khatri, J. Kavosi, M. Naraghi, Carbon nanotubes within Polymer Matrix can Synergistically Enhance Mechanical Energy Dissipation., Nanotechnology. (2018). doi:10.1088/1361-6528/aaa7e6.

[16] S.A. Suarez, R.F. Gibson, C.T. Sun, S.K. Chaturvedi, The influence of fiber length and fiber orientation on damping and stiffness of polymer composite materials, Exp. Mech. 26 (1986) 175–184. doi:10.1007/BF02320012.

[17] V. Singh, D. Joung, L. Zhai, S. Das, S.I. Khondaker, S. Seal, Graphene based materials: Past, present and future, Prog. Mater. Sci. 56 (2011) 1178–1271. doi:10.1016/j.pmatsci.2011.03.003.

[18] G. Mittal, V. Dhand, K.Y. Rhee, S.J. Park, W.R. Lee, A review on carbon nanotubes and graphene as fillers in reinforced polymer nanocomposites, J. Ind. Eng. Chem. 21 (2015) 11–25. doi:10.1016/j.jiec.2014.03.022.

[19] C. Lee, X. Wei, J.W. Kysar, J. Hone, Measurement of the elastic properties and intrinsic strength of monolayer graphene., Science. 321 (2008) 385–8. doi:10.1126/science.1157996.

[20] K. Hu, D.D. Kulkarni, I. Choi, V. V. Tsukruk, Graphene-polymer nanocomposites for structural and functional applications, Prog. Polym. Sci. 39 (2014) 1934–1972. doi:10.1016/j.progpolymsci.2014.03.001.

[21] J.R. Potts, D.R. Dreyer, C.W. Bielawski, R.S. Ruoff, Graphene-based polymer nanocomposites, Polymer (Guildf). 52 (2011) 5–25. doi:10.1016/j.polymer.2010.11.042.

[22] D.G. Papageorgiou, I.A. Kinloch, R.J. Young, Graphene/elastomer nanocomposites, Carbon N. Y. 95 (2015) 460–484. doi:10.1016/j.carbon.2015.08.055.

[23] R.J. Young, I.A. Kinloch, L. Gong, K.S. Novoselov, The mechanics of graphene

nanocomposites: A review, Compos. Sci. Technol. 72 (2012) 1459–1476. doi:10.1016/j.compscitech.2012.05.005.

[24] C. Soldano, A. Mahmood, E. Dujardin, Production, properties and potential of graphene, Carbon N. Y. 48 (2010) 2127–2150. doi:10.1016/j.carbon.2010.01.058.

[25] S. Stankovich, D.A. Dikin, G.H.B. Dommett, K.M. Kohlhaas, E.J. Zimney, E.A. Stach, R.D. Piner, S.B.T. Nguyen, R.S. Ruoff, Graphene-based composite materials, Nature. 442 (2006) 282–286. doi:10.1038/nature04969.

[26] A.K.Geim, K.S.Novolesov, Rise of graphene, Nat. Mater. 6 (2007) 183–191. doi:10.1038/nmat1849.

[27] I. Srivastava, R.J. Mehta, Z.Z. Yu, L. Schadler, N. Koratkar, Raman study of interfacial load transfer in graphene nanocomposites, Appl. Phys. Lett. 98 (2011) 10–13. doi:10.1063/1.3552685.

[28] M. a Rafiee, J. Rafiee, Z. Wang, H. Song, Z. Yu, N. Koratkar, Enhanced Mechanical Properties of Nanocomposites at Low Graphene Content, ACS Nano. 3 (2009) 3884–3890. doi:10.1021/nn9010472.

[29] L. Gong, I.A. Kinloch, R.J. Young, I. Riaz, R. Jalil, K.S. Novoselov, Interfacial stress transfer in a graphene monolayer nanocomposite, Adv. Mater. 22 (2010) 2694–2697. doi:10.1002/adma.200904264.

[30] P.M. Ajayan, J. Suhr, N. Koratkar, Utilizing interfaces in carbon nanotube reinforced polymer composites for structural damping, J. Mater. Sci. 41 (2006) 7824–7829. doi:10.1007/s10853-006-0693-4.

[31] P. Xu, J. Loomis, R.D. Bradshaw, B. Panchapakesan, Load transfer and mechanical

properties of chemically reduced graphene reinforcements in polymer composites, Nanotechnology. 23 (2012). doi:10.1088/0957-4484/23/50/505713.

[32] Y.-H. Yu, Y.-Y. Lin, C.-H. Lin, C.-C. Chan, Y.-C. Huang, High-performance polystyrene/graphene-based nanocomposites with excellent anti-corrosion properties, Polym. Chem. 5 (2014) 535–550. doi:10.1039/C3PY00825H.

[33] X. Wang, D. Tan, Z. Chu, L. Chen, X. Chen, J. Zhao, G. Chen, Mechanical properties of polymer composites reinforced by functionalized graphene prepared via direct exfoliation of graphite flakes in styrene, RSC Adv. 6 (2016) 112486–112492. doi:10.1039/c6ra24479c.

[34] B. Chen, N. Ma, X. Bai, H. Zhang, Y. Zhang, Effects of graphene oxide on surface energy, mechanical, damping and thermal properties of ethylene-propylene-diene rubber/petroleum resin blends, RSC Adv. 2 (2012) 4683. doi:10.1039/c2ra01212j.

[35] H. Kim, Y. Miura, C.W. MacOsko, Graphene/polyurethane nanocomposites for improved gas barrier and electrical conductivity, Chem. Mater. 22 (2010) 3441–3450. doi:10.1021/cm100477v.

[36] K. Hu, D.D. Kulkarni, I. Choi, V. V. Tsukruk, Graphene-polymer nanocomposites for structural and functional applications, Prog. Polym. Sci. 39 (2014) 1934–1972. doi:10.1016/J.PROGPOLYMSCI.2014.03.001.

[37] F. Hussain, M. Hojjati, M. Okamoto, R.E. Gorga, Review article: Polymer-matrix nanocomposites, processing, manufacturing, and application: An overview, J. Compos. Mater. 40 (2006) 1511–1575. doi:10.1177/0021998306067321.

[38] T. Kuilla, S. Bhadra, D. Yao, N.H. Kim, S. Bose, J.H. Lee, Recent advances in

graphene based polymer composites, Prog. Polym. Sci. 35 (2010) 1350–1375. doi:10.1016/j.progpolymsci.2010.07.005.

[39] M. Alexandre, P. Dubois, Polymer layered silicate nanocomposites preparation properties, Mater. Sci. Eng. 28 (2000) 1–63. doi:10.1002/1439-2054(20000601)279:1<1::AID-MAME1>3.0.CO;2-Q.

[40] B. Glaz, J. Riddick, E. Habtour, H. Kang, Interfacial Strain Energy Dissipation in Hybrid Nanocomposite Beams Under Axial Strain Fields, AIAA J. 53 (2015) 1544–1554. doi:10.2514/1.J053390.

[41] H. L. Cox, The elasticity and strength of paper and other fibrous materials, Br. J. Appl. Phys. 3 (1952) 72–79.

[42] T. Jiang, R. Huang, Y. Zhu, Interfacial sliding and buckling of monolayer graphene on a stretchable substrate, Adv. Funct. Mater. 24 (2014) 396–402. doi:10.1002/adfm.201301999.

[43] D.J. Nelson, J.W. Hancock, Interfacial slip and damping in fibre reinforced composites, J. Mater. Sci. 13 (1978) 2429–2440. doi:10.1007/BF00808058.

[44] Graphene Nanoplatelets and Single Layer Graphene Technical Data Sheet | ACS Material, (n.d.). https://www.acsmaterial.com/materials/graphene-series.html (accessed April 23, 2019).

[45] G. Wang, Z. Dai, Y. Wang, P. Tan, L. Liu, Z. Xu, Y. Wei, R. Huang, Z. Zhang, Measuring interlayer shear stress in bilayer graphene, Phys. Rev. Lett. 119 (2017) 1–7. doi:10.1103/PhysRevLett.119.036101.

[46] W. Dou, C. Xu, J. Guo, H. Du, W. Qiu, T. Xue, Y. Kang, Q. Zhang, Interfacial

Mechanical Properties of Double-Layer Graphene with Consideration of the Effect of Stacking Mode, ACS Appl. Mater. Interfaces. 10 (2018) 44941–44949. doi:10.1021/acsami.8b18982.

[47] F. Gardea, B. Glaz, J. Riddick, D.C. Lagoudas, M. Naraghi, Identification of energy dissipation mechanisms in CNT-reinforced nanocomposites, Nanotechnology. 27 (2016). doi:10.1088/0957-4484/27/10/105707.

[48] J.S. Cameron, D.S. Ashley, J.S. Andrew, G.S. Joseph, T.G. Christopher, Accurate thickness measurement of graphene, Nanotechnology. 27 (2016) 125704. http://stacks.iop.org/0957-4484/27/i=12/a=125704.

[49] Z. Li, I.A. Kinloch, R.J. Young, K.S. Novoselov, G. Anagnostopoulos, J. Parthenios, C. Galiotis, K. Papagelis, C.Y. Lu, L. Britnell, Deformation of Wrinkled Graphene, ACS Nano. 9 (2015) 3917–3925. doi:10.1021/nn507202c.

[50] G. Guo, Y. Zhu, Cohesive-Shear-Lag Modeling of Interfacial Stress Transfer Between a Monolayer Graphene and a Polymer Substrate, J. Appl. Mech. 82 (2015) 031005. doi:10.1115/1.4029635.

[51] C. Xu, T. Xue, W. Qiu, Y. Kang, Size Effect of the Interfacial Mechanical Behavior of Graphene on a Stretchable Substrate, ACS Appl. Mater. Interfaces. 8 (2016) 27099–27106. doi:10.1021/acsami.6b08812.

[52] T. Filleter, J.L. McChesney, A. Bostwick, E. Rotenberg, K. V. Emtsev, T. Seyller, K. Horn, R. Bennewitz, Friction and dissipation in epitaxial graphene films, Phys. Rev. Lett. 102 (2009) 1–4. doi:10.1103/PhysRevLett.102.086102.

[53] C. Lee, X. Wei, Q. Li, R. Carpick, J.W. Kysar, J. Hone, Elastic and frictional

properties of graphene, Phys. Status Solidi. 246 (2009) 2562–2567. doi:10.1002/pssb.200982329.

[54] O. Frank, M. Bouša, I. Riaz, R. Jalil, K.S. Novoselov, G. Tsoukleri, J. Parthenios, L. Kavan, K. Papagelis, C. Galiotis, Phonon and structural changes in deformed bernal stacked bilayer graphene, Nano Lett. 12 (2012) 687–693. doi:10.1021/nl203565p.

[55] C. Androulidakis, E.N. Koukaras, J. Rahova, K. Sampathkumar, J. Parthenios, K. Papagelis, O. Frank, C. Galiotis, Wrinkled Few-Layer Graphene as Highly Efficient Load Bearer, ACS Appl. Mater. Interfaces. 9 (2017) 26593–26601. doi:10.1021/acsami.7b07547.

[56] T.M.G. Mohiuddin, A. Lombardo, R.R. Nair, A. Bonetti, G. Savini, R. Jalil, N. Bonini, D.M. Basko, C. Galiotis, N. Marzari, K.S. Novoselov, A.K. Geim, A.C. Ferrari, Uniaxial strain in graphene by Raman spectroscopy: G peak splitting, Grüneisen parameters, and sample orientation, Phys. Rev. B - Condens. Matter Mater. Phys. 79 (2009) 1–8. doi:10.1103/PhysRevB.79.205433.

[57] F. Liu, N. Hu, H. Ning, Y. Liu, Y. Li, L. Wu, Molecular dynamics simulation on interfacial mechanical properties of polymer nanocomposites with wrinkled graphene, Comput. Mater. Sci. 108 (2015) 160–167. doi:10.1016/j.commatsci.2015.06.023.

[58] R. Kopp, F. Gardea, B.J. Glaz, E.C. Smith, Multi-fidelity Modeling of Interfacial Micromechanics for Off-Aligned Polymer/Carbon Nanotube Nanocomposites, in: 58th AIAA/ASCE/AHS/ASC Struct. Struct. Dyn. Mater. Conf., American Institute

of Aeronautics and Astronautics, Reston, Virginia, 2017: pp. 1–30. doi:10.2514/6.2017-1982.